Molecular Wrench Activity of DNA Helicases: Keys to Modulation of Rapid Kinetics in DNA Repair

Ashan Wettasinghe,[1] Melodee O. Seifi,[1] Marco Bravo,[2] Austen C. Adams,[1] Aman Patel,[1] Monica Lou,[1] Dimithree Kahanda,[1] Hao-Che Peng,[3] Allison L. Stelling,[3] Li Fan,[3] and Jason D. Slinker[1,3,4*]*

[1]Department of Physics, The University of Texas at Dallas, 800 W. Campbell Rd., SCI 10, Richardson, TX 75080.

[2]Department of Biochemistry, University of California, 900 University Ave, Riverside, CA 92521.

[3]Department of Chemistry, The University of Texas at Dallas, 800 W. Campbell Rd., SCI 10, Richardson, TX 75080.

[4]Department of Materials Science and Engineering, The University of Texas at Dallas, 800 W. Campbell Rd., SCI10, Richardson, TX 75080

Corresponding authors:

*Li Fan, Department of Biochemistry, University of California, 900 University Ave, Riverside, CA 92521. Phone: 951-827-3630. Fax: 951-827-4434. E-mail: li.fan@ucr.edu.

*Jason Slinker, The University of Texas at Dallas, 800 W. Campbell Rd., SCI 10, Richardson, TX 75080. Phone: 972-883-6513. Fax: 972-883-2848. E-mail: slinker@utdallas.edu.

Running title: Modulating DNA Helicase Molecular Wrench Activity

Manuscript total pages: 20

Manuscript total figures: 7

Supplementary Material total pages: 11

Supplementary Material total figures: 6

Supplementary Material total tables: 2

Supplementary Material description: Example SWV curves, control experiment for ATP addition, control experiment for DNA unzipping, summarized time constants, summarized binding dissociation constants, investigation by intrasweep square wave voltammetry (ISWV), illustration of DNA and kinetic rates, ATP reaction by conventional SWV, ATP reaction by ISWV.

Supplementary Material filename: SM_molwrench_7.pdf

Abstract: DNA helicase activity is essential for the vital DNA metabolic processes of recombination, replication, transcription, translation, and repair. Recently, an unexpected, rapid exponential ATP-stimulated DNA unwinding rate was observed from an *Archaeoglobus fulgidus* helicase (AfXPB) as compared to the slower conventional helicases from *Sulfolobus tokodaii,* StXPB1 and StXPB2. This unusual rapid activity suggests a "molecular wrench" mechanism arising from the torque applied by AfXPB on the duplex structure in transitioning from open to closed conformations. However, much remains to be understood. Here, we investigate the concentration dependence of DNA helicase binding and ATP-stimulated kinetics of StXPB2 and AfXPB, as well as their binding and activity in Bax1 complexes, via an electrochemical assay with redox-active DNA monolayers. StXPB2 ATP-stimulated activity is concentration-independent from 8 nM to 200 nM. Unexpectedly, AfXPB activity is concentration-dependent in this range, with exponential rate constants varying from seconds at concentrations greater than 20 nM to thousands of seconds at lower concentrations. At 20 nM, rapid exponential signal decay ensues, linearly reverses, and resumes with a slower exponential decay. This change in AfXPB activity as a function of its concentration is rationalized as the crossover between the fast molecular wrench and slower conventional helicase modes. AfXPB-Bax1 inhibits rapid activity, whereas the StXPB2-Bax1 complex induces rapid kinetics at higher concentrations. This activity is rationalized with the crystal structures of these complexes. These findings illuminate the different physical models governing molecular wrench activity for improved biological insight into a key factor in DNA repair.

Keywords: Base excision repair, Nucleotide excision repair, Xeroderma pigmentosum type B

Importance: We find that the DNA unwinding rate of a DNA helicase is concentration-dependent, transitioning between fast and slow modes near a threshold concentration. These rates reflect a conventional zipper slow mode and a fast mode, possibly due to a "molecular wrench" mechanism where the helicase separates the DNA by splaying out. We also find that binding partners modulate these rates to speed up or slow down helicase unwinding kinetics.

1. Introduction

Bolstered by their ability to unpack genetic material, helicases are widely regarded as vital to all organisms. Helicases are ubiquitous enzymes important for all RNA and DNA metabolism, including DNA replication, repair, transcription, and translation. Helicases are motor proteins that move directionally along nucleic acids to separate the strands as catalyzed by NTP hydrolysis (Raney 2013). DNA replication, recombination, transcription, translation, and repair are initiated by helicase activity (Gorbalenya and Koonin 1993; Patel and Picha 2000; Pyle 2008; Singleton et al. 2007; Sun and Wang 2016). While strides have been made in understanding their mechanisms for DNA unzipping, given the sheer number, structural heterogeneity, diversified functionality, and cooperative activity of helicases, extensive functional and structural studies are still required (Lohman et al. 2008) for a complete physical picture of this essential activity.

Xeroderma pigmentosum group B (XPB), a DNA helicase belonging to superfamily 2, exhibits DNA repair and transcription activity (Fan et al. 2006; Schultz et al. 2000). In nucleotide excision repair (NER), XPB unwinds the DNA duplex around the damaged site. XPB also initiates RNA polymerase II transcription by dehybridizing gene promoters (Gillet and Scharer 2006; Schaeffer et al. 1993). Disorders such as Cockayne syndrome, xeroderma pigmentosum, and trichothiodystrophy arise from XPB mutations (DiGiovanna and Kraemer 2012). While recent biochemical and structural research (Fan and DuPrez 2015; Fishburn et al. 2015; He et al. 2016; Kim et al. 2000; Rand et al. 2000) has led to mechanistic hypotheses for DNA unwinding by helicases, further study into the binding and activity of XPB is needed to elucidate its roles in transcription and repair.

Recently, we revealed a distinct new mode of helicase action, termed molecular wrench activity, applied by XPB to unwind DNA (Kahanda et al. 2018). As illustrated in Figure 1, a conventional helicase translocates along the DNA, sequentially breaking the hydrogen bonds between the base pairs. This process is driven by ATP hydrolysis and leads to the complete dehybridization of the duplex. We studied the *Sulfolobus tokodaii* XPB homologs, StXPB1 and StXPB2, together with the *Archaeoglobus fulgidus* XPB (AfXPB) and their interactions with DNA monolayers. DNA unwinding by StXPB1 and StXPB2 took tens of minutes, in line with prior ensemble fluorescence studies (Jang et al. 2010; Tani et al. 2010). Interestingly, the AfXPB helicase activity timescale, which had not been previously reported, was mere seconds. The different slow and fast decay functions of these distinct helicases may reflect two distinct modes of their DNA unwinding activity. Concomitantly, the crystal structures of StXPB2 and AfXPB revealed key differences in their conformations when complexed with DNA. While StXPB2 did not crystalize in a stable open structure, a stable open conformation was found for AfXPB. This finding of an open structure led to the postulate that AfXPB may stay in the open conformation after DNA binding. For AfXPB to adopt its active conformation with a closed ATP-binding groove, a 170° rotation between the two helicase domains is required, whereas StXBP2 needs only 50-80° rotations. Molecular wrench action commences when ATP binds to AfXPB and induces this open-to-closed domain rotation of the enzyme (Figure 1) that rapidly separates the two strands of the DNA duplex.

Both the conventional and molecular wrench modes of XPB activity are required for DNA repair: the molecular wrench conformational change can rapidly open the duplex strands at the damage site, while the conventional DNA helicase activity by XPB promotes broader unzipping and facilitates DNA bubble extension as mediated by XPD, another DNA helicase within the TFIIH complex. Our results showed that XPB is a faster helicase acting as a molecular wrench than a conventional helicase. This finding harmonizes with the biological role of XPB as the primary (likely the only) helicase to instigate duplex DNA opening at the damage site and as a secondary helicase (to XPD) to extend the DNA bubble for damage

incision. Furthermore, the slow kinetics of StXPBs reflect conventional DNA unzipping with XPB translocating along the DNA. In contrast, the fast decay function of AfXPB reflects the unique molecular wrench DNA unwinding activity by XPB (Figure 1) (Fan and DuPrez 2015).

The structural and kinetic signatures of this activity could profoundly influence DNA repair and transcription processes. The signature of molecular wrench activity was revealed with electrochemical DNA devices coupled with crystallography (Kahanda et al. 2018), which we will now leverage to discover the critical structural and chemical features that govern molecular wrench activity. Furthermore, AfXPB and StXPB have been shown to function with a binding partner, the endonuclease Bax1, which modulates the ATPase activity in opposite ways (Fan and DuPrez 2015). Further study of the DNA unwinding implications would clarify their overall role and function. Here, we utilize electrochemical experiments with DNA to track the binding and unzipping dynamics of conventional (StXBP2) and molecular wrench (AfXPB) helicase activity at various concentrations. In addition, we explore the concentration-dependent kinetics of these helicases and correlate these kinetics with their binding and structural features.

2. Results and Discussion

Electrochemical devices bearing double-stranded DNA monolayers were used to monitor DNA binding by the helicase and unwinding activity as previously described (Kahanda et al. 2018) and as illustrated in Figure 2. DNA bearing electrochemically-active Nile Blue redox probes (Gorodetsky et al. 2008b) were self-assembled onto gold electrodes on silicon chips (Slinker et al. 2010). In this configuration, the DNA provides an electronically coupled bridge for the surface-bound electrochemistry between the redox probes and the gold electrode (Drummond et al. 2003; Gorodetsky et al. 2008a) as facilitated by the network of overlapping π-orbitals of the DNA base stacking interactions (Arnold et al. 2016; Genereux and Barton 2010). Disruption of the DNA duplex structure lowers this signal by reducing the coupling between the electrode and the redox probe. The electrochemical signal from these redox-active DNA monolayers is recorded by square wave voltammetry (SWV), a technique sensitive to surface-bound Faradaic/electronic reactions (Osteryoung and Osteryoung 1985). Helicase binding disrupts the base hydrogen bonding and DNA suprastructure and lowers the peak current of the voltammetry peaks in proportion to the fraction of the monolayer bound. Our previous work showed that the binding of AfXPB or StXPB2 produced a disruption energetically equivalent to breaking a single A-T base pair (Kahanda et al. 2018). The addition of ATP initiates activity that breaks multiple base pair hydrogen bonds between the strands of the duplex, potentially fully dehybridizing the DNA and further reducing the signal. (The Nile blue strand is not tethered to the electrode once the DNA is dehybridized.) Assays were performed at room temperature.

Figure 3 shows the impact of ATP-induced helicase activity on these electrochemical DNA monolayers at 8 nM and 200 nM concentrations of the helicases. The helicases were first added to the electrochemically active DNA monolayers, and the initial binding reaction was allowed to reach equilibrium for at least 20 min. Then, 2 mM ATP was added to the reaction mixture to initiate the unwinding reaction. In Figure 3A, the conventional StXPB2 induces a continuous monoexponential decrease in the SWV peak current observed at both concentrations. Each curve was fitted with a first-order exponential of the form $Ae^{-t/\tau}$, where τ is the exponential time constant of the decay associated with separating the strands of the DNA duplexes across the complete DNA ensemble. The average exponential time constant τ_{ave} for the population was recorded over at least three trials for each StXPB2 concentration and found to be 5000 ± 1000 s and 2900 ± 500 s, respectively, for 8 nM and 200 nM concentrations. These reaction times are consistent with fluorescence studies of the helicase activity on ensembles of

DNA (Jang et al. 2010) and RNA (Tani et al. 2010) and our prior electrochemical experiment with the StXPB2 helicase (Kahanda et al. 2018). Thus, the timescale of activity, on the order of tens of minutes, is consistent with the conventional unzipping of an ensemble of DNA. The situation is more complex for the AfXPB helicase activity in Figure 3B. For the lower 8 nM concentration, ATP-stimulated AfXPB activity exhibited first-order exponential decay of the DNA electrochemistry, with an exponential time constant of τ_{ave} = 2400 ± 800 s, similar to the StXPB2 timescale associated with conventional activity. In sharp contrast, using a higher 200 nM concentration of AfXPB resulted in a much more rapid exponential decay time constant of 4 ± 2 s, nearly three orders of magnitude faster. This rapid decay is consistent with the timescale of our previous measure of AfXPB activity within experimental error (Kahanda et al. 2018) (at the lower concentration tested) and what we have ascribed as the characteristically fast kinetics of molecular wrench activity (Figures 1 and 2). Here, by testing lower and higher enzyme concentrations, we have revealed that ATP-stimulated AfXPB activity is concentration-dependent. These differing timescales of activity presumably alternate between conventional and molecular-wrench modalities.

To further understand the physical basis of these observed concentration-dependent kinetics, we measured the steady-state SWV peak current from electrochemical DNA monolayers versus the concentration of each helicase in the absence of ATP to measure helicase binding. As shown in Figure 4, each dataset shows sequential signal loss upon helicase addition, corresponding to the fraction of the DNA monolayer bound by the helicase. StXPB2 data were fit by a single Hill equation of the form:

$$S[H] = S_0 + (S_M - S_0)[H]^n / ([H_{1/2}]^n + [H]^n), \quad (1)$$

where $S[H]$ is the SWV signal loss at a particular concentration of helicase, S_0 is a baseline fit value, S_M is a maximum signal loss value, $[H]$ is the helicase concentration, $[H_{1/2}]$ is the helicase concentration at the midpoint of the signal change, and n is the Hill coefficient. For StXPB2, $H_{1/2}$, correlating with the binding dissociation constant K_D, was 158 nM, while n was 1.43, indicative of cooperative binding. Alternatively, close inspection of the AfXPB concentration dependence revealed a replicable deviation from a single binding isotherm by a dip in the data near 20 nM. This data was then fit by two simplified Langmuir binding isotherms (Esteban Fernandez de Avila et al. 2013; van de Weert and Stella 2011) of the form:

$$S[H] = S_0 - (S_0 - S_B)[H] / ([H] + K_D), \quad (2)$$

where $S([H])$ is the square wave peak height signal at a concentration $[H]$ of helicase, S_0 is the initial square wave peak height, S_B is the square wave background signal, and K_D is the binding dissociation constant associated with the system. From these fits, the lower concentration portion was fit with a tight K_{1D} = 25 nM, and the higher concentration portion was fit with a weaker K_{2D} = 334 nM. The details of this concentration-dependent binding curve can offer insights into the physical processes responsible for the concentration-dependent kinetics observed with ATP-stimulated AfXPB activity.

In Figure 5, we explored the ATP-stimulated AfXPB activity at three key concentrations displaying characteristic kinetics: 8 nM, 20 nM, and 40 nM. At the low concentration of 8 nM, as noted in Figure 3B, exponential decay is observed with slow dynamics corresponding to τ_{ave} = 2400 s. In contrast, at the highest concentration of 40 nM, rapid exponential decay is observed with τ_{ave} = 7.0 ± 0.5 s. This is the fast timescale associated with molecular wrench activity. Surprisingly, at the middle concentration of 20 nM AfXPB, a unique and replicable dynamic behavior is observed throughout the enzymatic reaction. Initially, a rapid exponential drop is

observed, with a τ_{1ave} = 6.2 ± 0.8 s. Yet, after this rapid initial decay, the SWV peak current does not drop fully to noise levels. After this, the current increases linearly with a slope m_{2ave} = 1.1 ± 0.2 %/s. (This is one of the relatively few examples of the recovery of the electrochemical DNA signal following enzymatic activity (Boon et al. 2002; DeRosa et al. 2005; Muren and Barton 2013).) Finally, on longer timescales, the signal again undergoes first-order exponential decay, with τ_{3ave} = 1600 ± 100 s. Overall, for 20 nM AfXPB, it appears that the DNA monolayer first experiences helicase molecular wrench activity, followed by recovery of the duplex and conventional unwinding activity by the helicase. Notably, this key concentration occurs precisely where there is a change in the slope—a "kink"—in the binding curve presented in Figure 4, where we have modeled the crossover between two binding isotherms. In our previous study, molecular wrench activity was observed at 10 nM AfXPB (Kahanda et al. 2018), indicating that ~10-20 nM is the crossover concentration range to observe these dynamic effects.

The question arises: what fundamental biochemical features induce such concentration-dependent AfXPB behavior and the characteristics of Figure 5D? Concerning the dynamic behavior of Figure 5D, We postulate that molecular wrench activity accounts for the rapid initial signal loss where present. We also assert that the two binding isotherms of Figure 4 correspond to two binding modes of the AfXPB helicase. Now, let us consider three distinct models, and while they are distinct, the activity may involve a combination of these views. i) Snap-back model: There have been several reports of a spring-loaded, slippage, or snap-back action of a range of DNA helicases, whereby they rebind to a previously scanned or unwound portion of the substrate with rapid DNA reannealing occurring (Myong 2005; Sun 2011; Wu 2017; Singh 2019; Le 2023). This can be facilitated by multiple binding sites on the monomer helicase, giving rise to separate affinity for ssDNA, dsDNA, DNA forks, or other features. ii) Catch-and-release model: We could be witnessing a modified catch-and-release model, whereby the helicase releases from DNA following molecular wrench activity and ATP-to-ADP hydrolysis and returns to DNA after rebinding to ATP apart from the DNA, thus bypassing molecular wrench activity. iii) Cooperative model: In this view, the initial step of molecular wrench helicase activity requires two AfXPB monomer helicases to be bound to the DNA. Once unzipping is accomplished, the helicases are released, and the DNA rehybridizes. When AfXPB rebinds, it can immediately process as a conventional monomeric helicase due to the excess of ATP (2 mM) compared to AfXPB (20 nM).

Now, let us consider key overall observations. At higher AfXPB concentrations (~40 nM or more), molecular wrench activity dominates and completely extinguishes the signal from the monolayer. For the dynamic intermediate concentration regime near 20 nM, the signal recovery is ~100 s. This is notably slower than the rehybridization single-molecule experiments, which are on the order of milliseconds to seconds (Myong 2005; Sun 2011; Wu 2017; Singh 2019; Le 2023). The slower timescale here follows from the recovery of the monolayer ensemble. It indicates a significant time between the end of the correlated initial unzipping activity and the initiation of the second set of unzipping events. The signal recovers to nearly 100% of the initial value, likely suggesting that the DNA strands were not completely dehybridized from the initial activity. Notably, the crossover to this dynamic intermediate regime at 20 nM correlates with a kink in the binding curve of Figure 4—the onset of the second binding isotherm. So, the rapid kinetics are initiated as an apparent second binding mode is activated, possibly corresponding to a binding partner. Carefully considered, these observations lend credence to each of the proposed models, and some combination of the models may give rise to the observed dynamic behavior.

Next, we investigated the binding and ATP-stimulated kinetics of StXPB2-Bax1 and AfXPB-Bax1 complexes. The Bax1 nuclease affects the conformation and activity of StXPB2 and AfXPB differently. Crystal structure and activity analyses have shown that StXPB2-Bax1

stabilizes StXPB2 in its closed conformation (Supporting Information Figure S4) and stimulates ATP hydrolysis, while AfXPB-Bax1 stabilizes AfXPB in the open conformation consistent with the crystal structure of the complex (Supporting Information Figure S5) and reduces its ATPase activity (DuPrez et al. 2020). We measured the concentration dependence of initial DNA binding and ATP-stimulated activity of StXPB2-Bax1 and AfXPB-Bax1 helicase-Bax1 complexes and presented the results in Figure 6. In Figures 6A and 6B, forming the complex with Bax1 shifts the binding activity of both helicases. For StXPB2-Bax1, the curve is fit with the simplified Langmuir binding isotherm of equation 2, with K_D = 640 nM. As expected, the binding of the StXPB2-Bax1 is lowered relative to StXPB2. For AfXPB-Bax1, the curve was fit with the Hill equation (equation 1), with a K_D of 145 nM and a Hill coefficient n of 2.2.

The ATP-stimulated kinetics of each complex at 10 nM and 200 nM are shown in Figures 6C and 6D. The kinetics of StXPB2-Bax1 are dynamic with concentration. The exponential time constant for the lower 10 nM concentration was similar to the time constants for uncomplexed StXPB2 (3500 s). However, the higher 200 nM concentration exhibits substantially more rapid activity. A monoexponential decay with τ_{ave} = 7.1 ± 0.8 s was observed at this concentration. In the complex, Bax1 stabilizes the active closed conformation of StXPB2 (See Supporting Information Figure S4) that enhances its ATPase activity (DuPrez et al. 2020). It is curious and noteworthy to see that this rapid timescale is similar to molecular wrench activity. For AfXPB-Bax1, while exponential signal loss is observed again, the activity rate is lowered for both concentrations, with the rapid molecular wrench activity completely suppressed at 200 nM (τ_{ave} = 3330 ± 70 s). This is consistent with the crystal structure of the complex (Supporting Information Figure S5) and the understanding of molecular wrench activity. An AfXPB conformational change from open to closed is requisite for rapid activity, and Bax1-binding may lower the propensity for this conformational change to occur, limiting the ATP activity rate.

Finally, as a particular note of caution for activity assays involving ATP, we show the impact of failing to account for the influence of ATP addition to the solution's pH. We noted that 2 mM ATP was sufficient to change the pH of our standard buffer solution to acidic conditions (pH 5-6), with catastrophic consequences for the DNA hybridization and composite self-assembled monolayer. (To correct this, we first dissolve the ATP in pH 10 buffer for all other experiments as noted in the methods.) Figure 7 shows the impact of 2 mM ATP on DNA electrochemistry in the absence of helicase when insufficient buffer conditions yield acidic reaction conditions. In Figure 7A, successive SWV curves were recorded before and after ATP addition. Once the ATP is added, no apparent voltammetry peak can be observed, and the voltammetry background increases significantly. The impact of the acidic conditions is rapid, with activity on the order of milliseconds. To view the details of this reaction in more detail, we added ATP during a voltammetry peak and noted the changes in Figure 7B. Initially, the current drops with the loss of the DNA electrochemistry from acid-induced DNA dehybridization. Subsequently, the signal increases dramatically as thiol reduction ensues, exposing the electrode to irreversible oxygen electrochemistry. In Figures 7C and 7D, we demonstrate how to precisely quantify the rapid DNA dehybridizing dynamics by subtracting a pre-addition averaged reference curve, enabling kinetic analysis with 16.7 ms resolution corresponding to the SWV period. The resulting linear decay curve in Figure 7D reveals a signal loss rate of 18.6 pA/ms or 49% of the DNA peak current per second. We term this technique intrasweep square wave voltammetry (ISWV) and discuss this method in detail in the Supporting Information.

3. Conclusion

We investigated the concentration dependence of DNA helicase binding and ATP-stimulated kinetics of StXPB2 and AfXPB, as well as their binding and activity in Bax1 complexes through electrochemistry with redox-active DNA monolayers. The timescale of StXPB2 ATP-stimulated DNA unzipping activity was concentration-independent from 8 nM to 200 nM and consistent with conventional helicase unwinding. Alternatively, AfXPB activity was highly concentration dependent in this range, with exponential rate constants varying from seconds to thousands of seconds. At 20 nM, rapid exponential decay of the electrochemical signal from the reaction was followed by linear recovery and subsequent slower exponential decay. This concentration-dependent AfXPB ATP activity is rationalized as the crossover between a rapid molecular wrench process and a slower conventional helicase mechanism. The AfXPB-Bax1 protein complex inhibited this fast ATPase activity. In contrast, the StXPB2-Bax1 complex induces rapid ATP-induced kinetics at higher concentrations of the enzymes. The crystal structures of these complexes rationalize this change in activity as a function of helicase concentration: AfBax1 stabilizes AfXPB in the inactive open conformations, whereas StXPB2-Bax1 stabilizes the active closed form of StXPB2. These findings illuminate the factors governing molecular wrench activity for improved biological insight into a key factor in DNA repair.

4. Materials and Methods

4.1 Protein expression and purification

AfXPB and AfXPB-Bax1 were expressed via published protocols (DuPrez et al. 2020; Fan et al. 2006). StXPB2 and StXPB2-Bax1 expressions followed published protocols (DuPrez et al. 2020; Ma et al. 2011). The expression plasmids pET15b/StXPB2 (Protein Accession number: WP_010979669) and pET15b/StBax1 (Protein Accession number: WP_010979670), generously provided by Dr. Yulong Shen at the Shandong University of China, were transformed into *E. coli* Rosetta (DE3) pLysS competent cells.

Helicase samples for electrochemistry studies were thawed and passed through a PD10 column (GE) for buffer exchange into 10 mM TrisCl pH 8, 200 mM NaCl, and 10 mM $MgCl_2$. Protein concentrations were determined by absorbance measurements at 280 nm before freezing in liquid nitrogen and shipment on dry ice.

4.2 Synthesis of DNA

Double-stranded DNA was prepared using the 17mer sequence 3'-CTCTATATTTCGTGCGT$_{NB}$-5' and its fully complementary sequence 5’-(C6 thiol)-GAGATATAAAGCACGCA-3’. These oligonucleotides were synthesized on an H-2 DNA Synthesizer from K & A Labs (Germany). T_{NB} denotes the position of the thymine modified with a Nile Blue redox probe. This probe-labeled base was formed by coupling Nile Blue perchlorate (Sigma Aldrich) with the 5-[3-acrylate NHS ester] deoxyuridine phosphoramidite from Glen Research. The dye was covalently coupled and processed under UltraMild conditions according to established procedures.(Gorodetsky et al. 2008b) The C6 thiol linker was coupled to the oligo as the Glen Research thiol-modifier C6 S-S phosphoramidite, and the dithiol was reduced for self-assembly.

4.3 Purification of DNA

All oligonucleotides were purified *via* two rounds of high-performance liquid chromatography (HPLC) on a Shimadzu LC-20AD instrument outfitted with a SIL-20A autosampler and an SPD-M20A diode array detector as previously described (McWilliams et al. 2015; Wohlgamuth et al. 2014). The identity of the desired products was confirmed by matrix-assisted laser desorption ionization time-of-flight mass spectrometry (MALDI-TOF) on a Shimadzu Axima Confidence mass spectrometer.

4.4 Preparation of the double-stranded DNA

The oligonucleotides were quantified *via* UV-visible spectroscopy on a Beckman DU-800 UV-visible spectrophotometer. The formation of duplex DNA was verified by temperature-dependent absorbance measurements with melting temperature analysis.

4.5 Fabrication of Devices

The chips/substrates featuring multiplexed gold electrodes for DNA self-assembly and electrochemical experiments were prepared as previously described (McWilliams et al. 2015; Slinker et al. 2010).

4.6 Self-Assembly of DNA Monolayers

The DNA monolayers were self-assembled onto gold electrode pads from a solution with 25 μM of the duplex DNA, 5 mM phosphate, 50 mM sodium chloride, pH = 7 buffer solution over 12 h to 18 h. The substrates were backfilled with mercaptohexanol for 1 h to remove nonspecifically bound DNA and then thoroughly rinsed with buffer to remove residual mercaptohexanol.

4.7 Electrochemical measurements on DNA monolayers

The multiplexed substrates were placed in a custom mount and connected to electrochemical testing hardware (a CH Instruments CHI730D Electrochemical Analyzer and a CHI 684 Multiplexer). Square wave voltammetry was generally performed at 40 Hz with a 0.025 mV amplitude and 4 mV increment. The electrochemical measurements were performed in pH 7.9 buffer containing 50 mM NaCl, 10 mM Tris-HCl, 10 mM $MgCl_2$, and 4 mM spermidine. For helicase binding experiments, helicases were added to this solution and allowed to equilibrate for at least 20 min, and SWV was recorded under the helicase incubation solution. For kinetics experiments, helicases were first added to the solution and allowed to equilibrate for at least 20 min. Then, ATP was added to this helicase incubation solution, and the SWV signal was recorded over time with ATP and helicase present. The ATP solution was prepared at pH 10 buffer as above for ATP experiments to ensure a pH of ~7.9 after ATP addition. See Supporting Information Figure S1-S3 for example electrochemistry and controls of this data. For details of the ISWV experiment (Figure 7), please see the Supporting Information.

Supporting Information

Supporting Information is available from the Wiley Online Library or from the author. Example SWV curves, control experiment for ATP addition, control experiment for DNA unzipping, summarized time constants, summarized binding dissociation constants, crystal structures for helicase-Bax1 complexes, investigation by intrasweep square wave voltammetry (ISWV), illustration of DNA and kinetic rates, ATP reaction by conventional SWV, ATP reaction by ISWV. Filename: SM_molwrench_8.pdf.

Conflict of Interests Statement

The authors declare no conflicts of interest.

Data Availability Statement

The data is available from the authors on reasonable request.

Acknowledgements

This work was funded by NIH grant number R01GM108893, Office of Naval Research grant number N00014-16-1-2741, and Welch Foundation grant number AT-2079-20210327.

References

Arnold AR, Grodick MA, Barton JK (2016) DNA charge transport: From chemical principles to the cell. Cell Chem Biol. 23(1):183-197.

Boon EM, Salas JE, Barton JK (2002) An electrical probe of protein-DNA interactions on DNA-modified surfaces. Nat Biotechnol. 20(3):282-286.

DeRosa MC, Sancar A, Barton JK (2005) Electrically monitoring DNA repair by photolyase. Proc Natl Acad Sci U S A. 102(31):10788-10792.

DiGiovanna JJ, Kraemer KH (2012) Shining a light on xeroderma pigmentosum. J Invest Dermatol. 132(3):785-796.

Drummond TG, Hill MG, Barton JK (2003) Electrochemical DNA sensors. Nat Biotechnol. 21(10):1192-1199.

DuPrez K, He F, Chen Z, Hilario E, Fan L (2020) Structural basis of the xpb–bax1 complex as a dynamic helicase–nuclease machinery for DNA repair. Nucleic Acids Res. 48(11):6326-6339.

Esteban Fernandez de Avila B, Watkins HM, Pingarron JM, Plaxco KW, Palleschi G, Ricci F (2013) Determinants of the detection limit and specificity of surface-based biosensors. Anal Chem. 85(14):6593-6597.

Fan L, Arvai AS, Cooper PK, Iwai S, Hanaoka F, Tainer JA (2006) Conserved xpb core structure and motifs for DNA unwinding: Implications for pathway selection of transcription or excision repair. Mol Cell. 22(1):27-37.

Fan L, DuPrez KT (2015) Xpb: An unconventional sf2 DNA helicase. Prog Biophys Mol Biol. 117(2-3):174-181.

Fishburn J, Tomko E, Galburt E, Hahn S (2015) Double-stranded DNA translocase activity of transcription factor tfiih and the mechanism of rna polymerase ii open complex formation. Proc Natl Acad Sci U S A. 112(13):3961-3966.

Genereux JC, Barton JK (2010) Mechanisms for DNA charge transport. Chem Rev. 110(3):1642-1662.

Gillet LCJ, Scharer OD (2006) Molecular mechanisms of mammalian global genome nucleotide excision repair. Chem Rev. 106(2):253-276.

Gorbalenya AE, Koonin EV (1993) Helicases: Amino acid sequence comparisons and structure-function relationships. Curr Opin Struct Biol. 3(3):419-429.

Gorodetsky AA, Buzzeo MC, Barton JK (2008a) DNA-mediated electrochemistry. Bioconjucate Chem. 19(12):2285-2296.

Gorodetsky AA, Ebrahim A, Barton JK (2008b) Electrical detection of tata binding protein at DNA-modified microelectrodes. J Am Chem Soc. 130(10):2924-2925.

He Y, Yan CL, Fang J, Inouye C, Tjian R, Ivanov I, Nogales E (2016) Near-atomic resolution visualization of human transcription promoter opening. Nature. 533(7603):359-+.

Jang H, Kim YK, Kwon HM, Yeo WS, Kim DE, Min DH (2010) A graphene-based platform for the assay by helicase. Angew Chem-Int Edit. 49(33):5703-5707.

Kahanda D, DuPrez KT, Hilario E, McWilliams MA, Wohlgamuth CH, Fan L, Slinker JD (2018) Application of electrochemical devices to characterize the dynamic actions of helicases on DNA. Anal Chem. 90(3):2178-2185.

Kim TK, Ebright RH, Reinberg D (2000) Mechanism of atp-dependent promoter melting by transcription factor iih. Science. 288(5470):1418-1421.

Le ST, Choi S, Lee S-W, Kim H, Ahn B (2023) ssDNA reeling is an intermediate step in the reiterative DNA unwinding activity of the WRN-1 helicase. J Biol Chem 299.

Lohman TM, Tomko EJ, Wu CG (2008) Non-hexameric DNA helicases and translocases: Mechanisms and regulation. Nat Rev Mol Cell Biol. 9(5):391-401.

Ma XQ, Hong Y, Han WY, Sheng DH, Ni JF, Hou GH, Shen YL (2011) Single-stranded DNA binding activity of xpbi, but not xpbii, from sulfolobus tokodaii causes double-stranded DNA melting. Extremophiles. 15(1):67-76.

Myong S, Rasnik I, Joo C, Lohman TM, Ha T (2005) Repetitive shuttling of a motor protein on DNA. Nature 437:1321-1325.

McWilliams MA, Bhui R, Taylor DW, Slinker JD (2015) The electronic influence of abasic sites in DNA. J Am Chem Soc. 137:11150–11155.

Muren NB, Barton JK (2013) Electrochemical assay for the signal-on detection of human DNA methyltransferase activity. J Am Chem Soc. 135(44):16632-16640.

Osteryoung JG, Osteryoung RA (1985) Square-wave voltammetry. Anal Chem. 57(1):101-110.

Patel SS, Picha KM (2000) Structure and function of hexameric helicases. Annu Rev Biochem. 69:651-697.

Pyle AM. 2008. Translocation and unwinding mechanisms of rna and DNA helicases. Annual review of biophysics. Palo Alto: Annual Reviews. p. 317-336.

Rand MD, Grimm LM, Artavanis-Tsakonas S, Patriub V, Blacklow SC, Sklar J, Aster JC (2000) Calcium depletion dissociates and activates heterodimeric notch receptors. Mol Cell Biol. 20(5):1825-1835.

Raney KD. 2013. Structure and function of sf1 DNA helicases. DNA helicases and DNA motor proteins. 1 ed. New York: Springer-Verlag.

Schaeffer L, Roy R, Humbert S, Moncollin V, Vermeulen W, Hoeijmakers JHJ, Chambon P, Egly JM (1993) DNA-repair helicase - a component of btf2 (tfiih) basic transcription factor. Science. 260(5104):58-63.

Schultz P, Fribourg S, Poterszman A, Mallouh V, Moras D, Egly JM (2000) Molecular structure of human tfiih. Cell. 102(5):599-607.

Singh SP, Soranno A, Sparks MA, Galletto R (2019) Branched unwinding mechanism of the Pif1 family of DNA helicases. Proceedings of the National Academy of Sciences 116:24533-24541.

Singleton MR, Dillingham MS, Wigley DB (2007) Structure and mechanism of helicases and nucleic acid translocases. Annu Rev Biochem. 76:23-50.

Slinker JD, Muren NB, Gorodetsky AA, Barton JK (2010) Multiplexed DNA-modified electrodes. J Am Chem Soc. 132(8):2769-2774.

Sun B, Wang MD (2016) Single-molecule perspectives on helicase mechanisms and functions. Critical reviews in biochemistry and molecular biology. 51(1):15-25.

Sun B, Johnson DS, Patel G, Smith BY, Pandey M, Patel SS, Wang MD (2011) ATP-induced helicase slippage reveals highly coordinated subunits. Nature 478:132-135.

Tani H, Fujita O, Furuta A, Matsuda Y, Miyata R, Akimitsu N, Tanaka J, Tsuneda S, Sekiguchi Y, Noda N (2010) Real-time monitoring of rna helicase activity using fluorescence resonance energy transfer in vitro. Biochem Biophys Res Commun. 393(1):131-136.

van de Weert M, Stella L (2011) Fluorescence quenching and ligand binding: A critical discussion of a popular methodology. J Mol Struct. 998(1-3):144-150.

Wohlgamuth CH, McWilliams MA, Mazaheripour A, Burke AM, Lin KY, Doan L, Slinker JD, Gorodetsky AA (2014) Electrochemistry of DNA mono layers modified with a perylenediimide base surrogate. J Phys Chem C. 118(50):29084-29090.

Wu WQ, Hou XM, Zhang B, Fossé P, René B, Mauffret O, Li M, Dou SX, Xi XG (2017) Single-molecule studies reveal reciprocating of WRN helicase core along ssDNA during DNA unwinding. Sci Rep 7:43954.

Figure 1. A) An illustration of conventional and molecular wrench helicase mechanisms for AfXPB. The domains of AfXPB are colored green and gray. B) Structural comparison of AfXPB and StXPB2. Center: AfXPB structure is superimposed with the two StXPB2 structures over the damage recognition domain and helicase domain1 (gray). For AfXPB, the C-terminal halves are shown as green in the open conformation and red in the closed conformation. For StXPB2, two open crystal structures are shown. The C-terminal halves are shown as cyan for structure A and magenta for structure B. The AfXPB closed conformation is a computational model, and the ATP-binding groove is highlighted. Reprinted (adapted) with permission from Anal Chem. 90(3):2178-2185. Copyright 2018 American Chemical Society.

Figure 2. Concept figure of electrochemical detection of helicase DNA binding and unzipping activity. Electrochemistry is recorded with the reduction of a Nile blue redox probe distal to the electrode and facilitated by the DNA. Binding activity lowers the signal in proportion to the fraction of monolayer bound, and ATP treatment further lowers the signal through the loss of the duplex.

Figure 3. ATP-initiated kinetics of StXPB2 and AfXPB helicases. A) Normalized SWV peak current vs. time after ATP addition for electrochemically active DNA monolayers treated with two concentrations of StXPB2 helicase. B) Normalized SWV peak current vs. time after ATP addition for electrochemically active DNA monolayers treated with two different concentrations of AfXPB helicase. (Inset: Normalized SWV peak current vs. time for the 200 nM AfXPB sample over the first 30 s.) Symbols indicate the data and solid curves are first-order exponential decay fits to the data, and decay times are presented as average ± standard error of the mean for at least three trials.

Figure 4. The concentration dependence of DNA binding of StXPB2 and AfXPB helicases. Normalized SWV peak current vs. helicase concentration. Symbols are data points, error bars represent the standard error of the mean for three trials, and the dashed lines represent fits to the data. (No ATP was added.)

Figure 5. Detailed ATP-stimulated kinetics of the AfXPB helicase. Normalized SWV peak current vs. time after ATP addition for electrochemically active DNA monolayers treated with various concentrations of AfXPB helicase. A) 8 nM AfXPB. B) 20 nM AfXPB. C) 40 nM AfXPB. D) 20 nM AfXPB, longer timescale. Symbols indicate the data, solid curves are first-order exponential decay fits to the data, and decay times are presented as average ± standard error of the mean for at least three trials.

Figure 6. Binding and kinetics of Helicase-BAX complexes. A) Normalized SWV peak current vs. helicase concentration for StXPB2 (Figure 4 data) and StXPB2-Bax1. (No ATP was added.) B) Normalized SWV peak current vs. helicase concentration for AfXPB (Figure 4 data) and AfXPB-Bax1. (No ATP was added.) C) Normalized SWV peak current vs. time after ATP addition for electrochemically active DNA monolayers treated with various concentrations of StXPB2-Bax1 helicase. D) Normalized SWV peak current vs. time after ATP addition for electrochemically active DNA monolayers treated with various concentrations of AfXPB-Bax1 helicase. Symbols indicate the data, solid curves are first-order exponential decay fits to the data, and decay times are presented as average ± standard error of the mean for at least three trials.

Figure 7. Catastrophic loss of DNA electrochemical signal under ATP-induced acidic conditions with insufficient buffering. A) Successive SWV sweeps before and after ATP addition. B) A SWV curve from 25 SWV scans before ATP addition (blue) and a curve recorded during ATP addition (red). C) The SWV curves of Figure 7B focused on the region between −0.120 and −0.212 V vs. Ag/AgCl. D) The difference in current between the red and blue curves of Figure 7C is plotted against time after ATP addition, showing the quantifiable rapid signal loss.

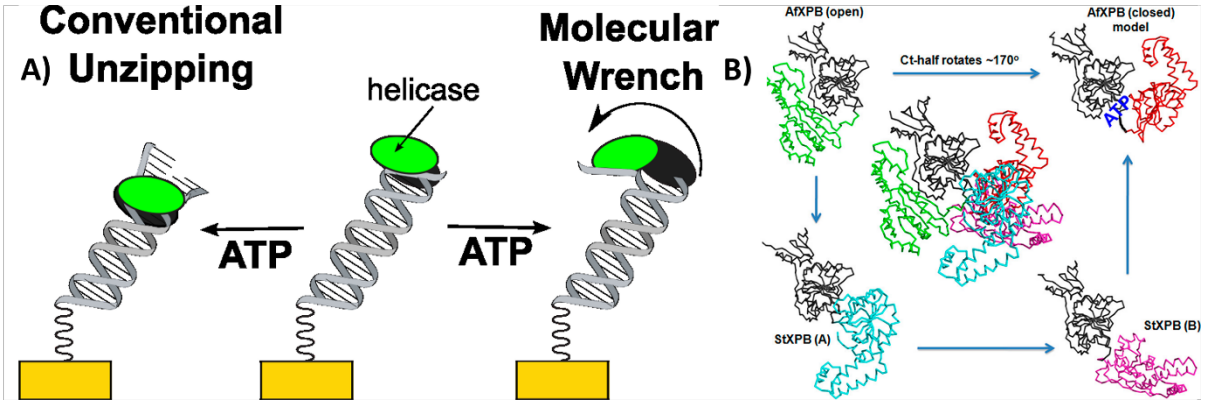

Figure 1

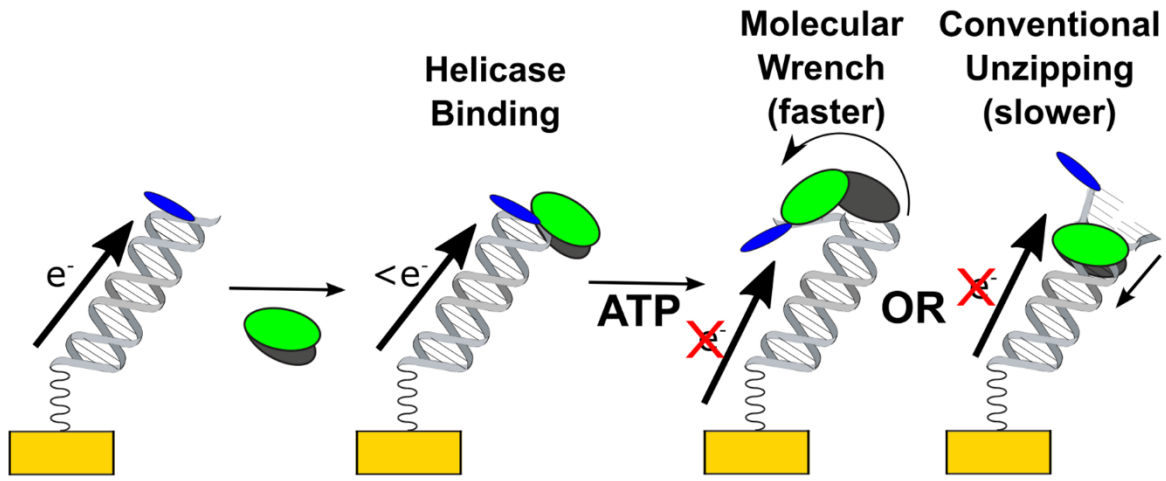

Figure 2

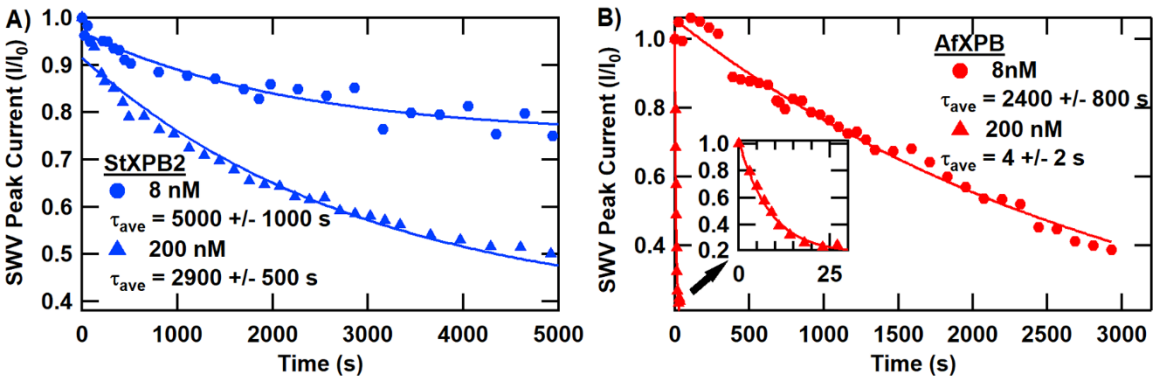

Figure 3

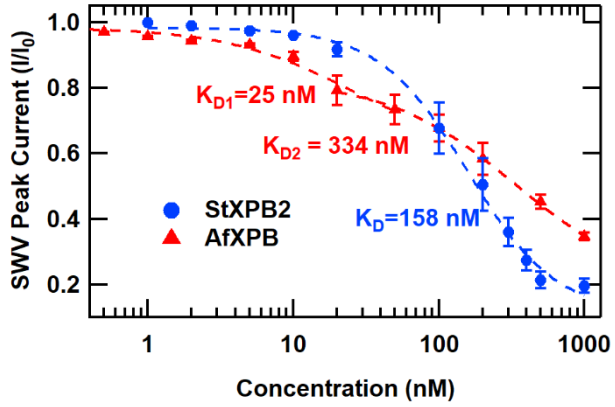

Figure 4

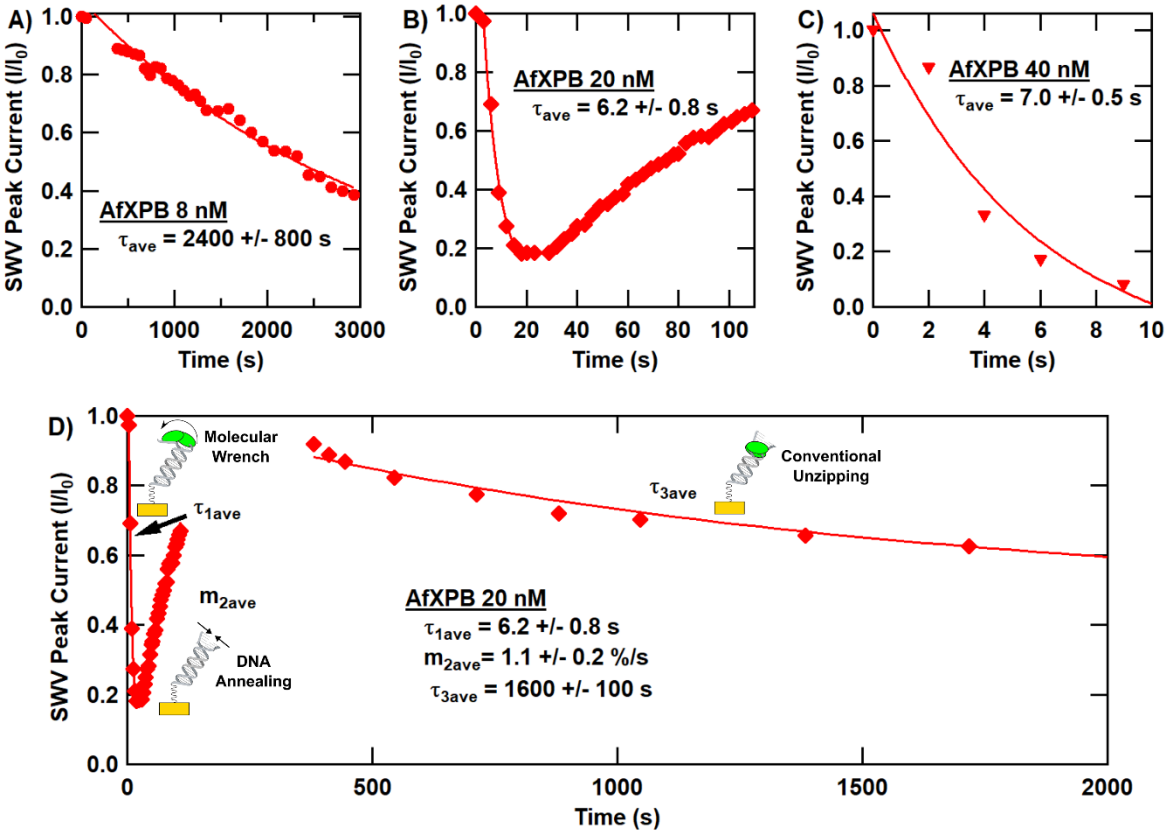

Figure 5

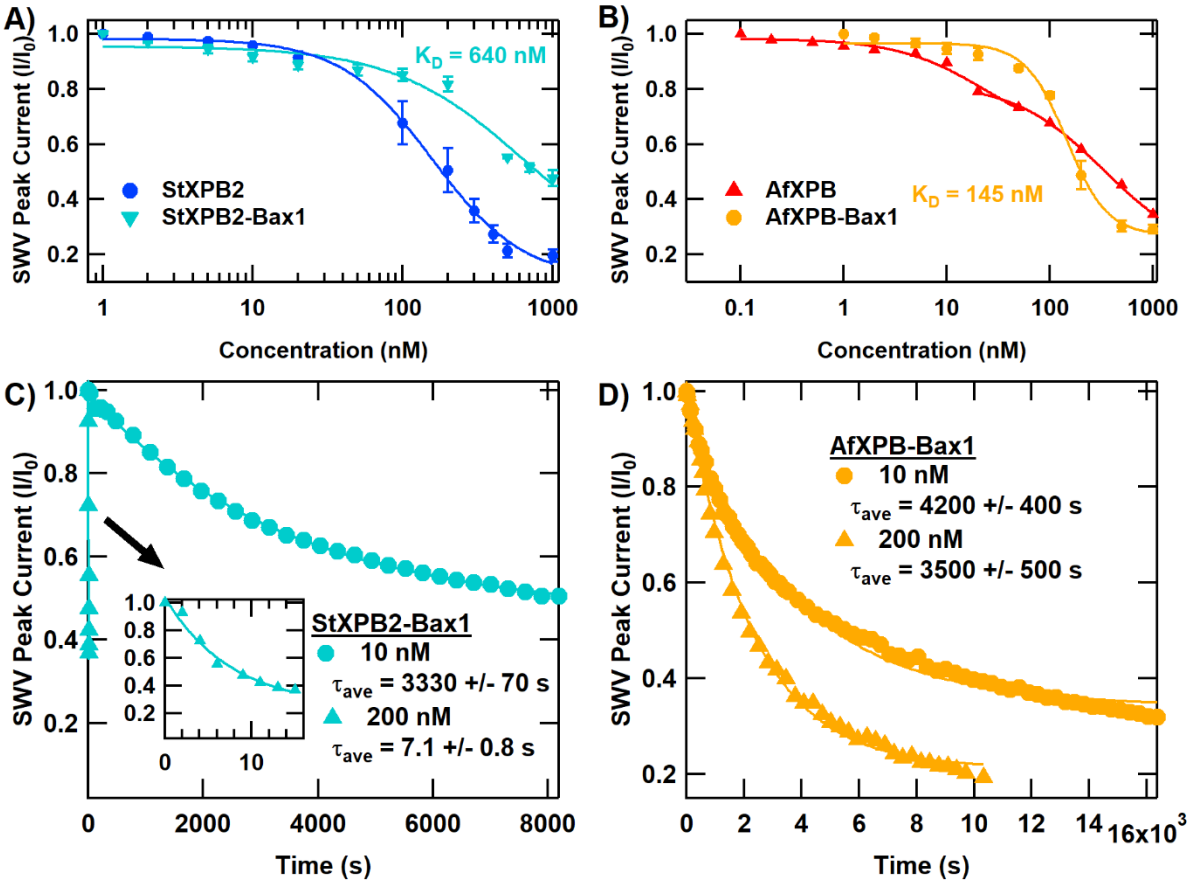

Figure 6

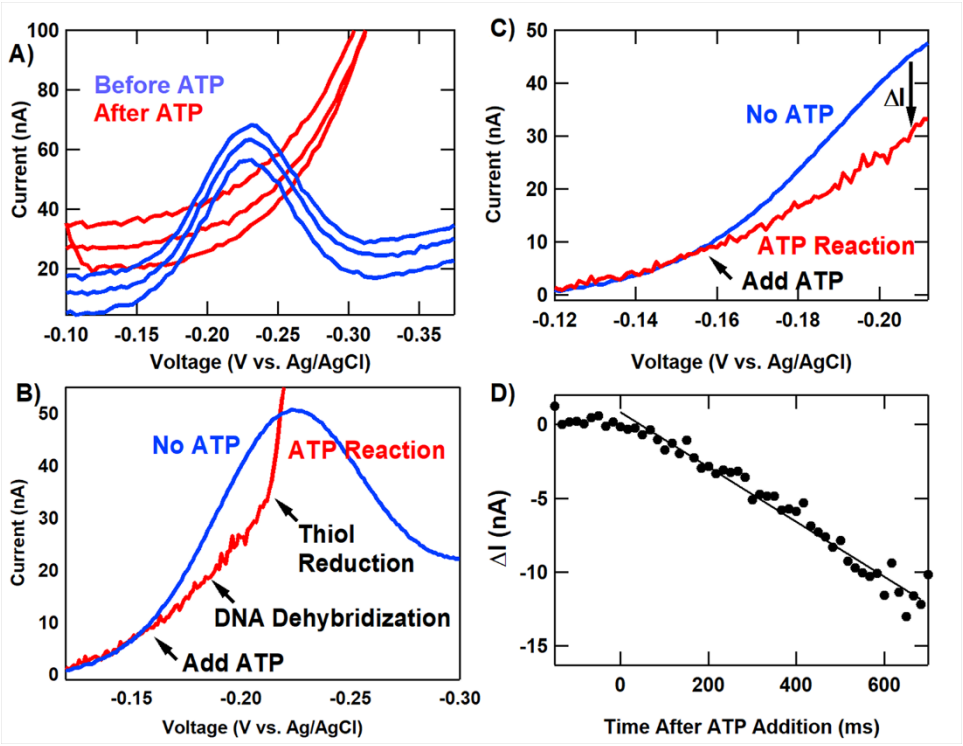

Figure 7